◆ Human Brain Mapping 20:41–49(2003) ◆

Directly Mapping Magnetic Field Effects of Neuronal Activity by Magnetic Resonance Imaging

Jinhu Xiong,* Peter T. Fox, and Jia-Hong Gao

Research Imaging Center, University of Texas Health Science Center at San Antonio, San Antonio, Texas

Abstract: Magnetic resonance imaging (MRI) of brain functional activity relies principally on changes in cerebral hemodynamics, which are more spatially and temporally distributed than the underlying neuronal activity changes. We present a novel MRI technique for mapping brain functional activity by directly detecting magnetic fields induced by neuronal firing. Using a well-established visuomotor paradigm, the locations and latencies of activations in visual, motor, and premotor cortices were imaged at a temporal resolution of 100 msec and a spatial resolution of 3 mm, and were found to be in consistent with the electrophysiological and functional MRI (fMRI) literature. Signal strength was comparable to traditional event-related fMRI methods: about 1% of the baseline signal. The magnetic-source MRI technique greatly increases the temporal accuracy in detecting neuronal activity, providing a powerful new tool for mapping brain functional organization in human and animals. *Hum. Brain Mapping 20:41–49, 2003.* © 2003 Wiley-Liss, Inc.

Key words: magnetic field effects; neuronal activity; fMRI; magnetic source imaging; motor cortex; visual cortex

INTRODUCTION

Advances in neural imaging techniques have enhanced greatly our understanding of functional organizations of the human brain. However, functional MRI (fMRI) technique used currently depends on measuring regional cerebral hemodynamics to infer neural activation, rather than directly detecting neuronal activity. As the relationship between neuronal activity and cerebral hemodynamics is not thoroughly understood, interpretations of the results are typically confounded by the coupling of neuronal activity and cerebral hemodynamics. Spatial and temporal resolutions of these measurements are also often limited by the complex vascular geometry and slow response function of cerebral hemodynamics, rather than physical limitations of the imaging methodologies. A much better solution for mapping brain activity is direct detection of electromagnetic sources originated from the neural firing using MRI.

Mapping neuronal activity with MRI by detecting neuronal magnetic fields is theoretically straightfor-

Contract grant sponsor: National Science Foundation; Contract grant number: BCS 0225711; Contract grant sponsor: National Institutes of Health; Contract grant numbers: RO1 MH067163, AG19844, RR17198.

*Correspondence to: Jinhu Xiong, PhD, Research Imaging Center, The University of Texas Health Science Center at San Antonio, 7703 Floyd Curl Drive, San Antonio, TX 78229-6240.
E-mail: xiong@uthscsa.edu

Received for publication 13 May 2003; Accepted 5 June 2003
DOI 10.1002/hbm.10124

ward, but practically challenging. The MRI signal is based on inducing and detecting phase-coherent nuclear spins. Nuclear spins exposed to neuronal magnetic fields will lose phase coherence, which will decrease MRI signal strength. It is well established by magnetoencephalography (MEG) that magnetic fields generated by cortical neuronal activity are detectable even at the scalp ($\sim 10^{-13}$ T) [Cohen, 1968]. Although the magnetic field at the source (the cerebral cortex) will necessarily be much stronger than at the scalp (2–4 cm away), it remains to be proven that the magnetic-source (ms) MRI effect is strong enough to be detectable and useful. MRI detection of weak, transient magnetic fields has been demonstrated in water phantoms [Bodurka et al., 1999; Bodurka and Bandettini, 2002; Scott et al., 1992] and even in the human body using externally applied currents [Joy et al., 1989]. An early attempt at direct mapping of neuronal activity was reported [Kamei et al., 1999], but has never been replicated. We present magnetic-field-effect modeling and experimental confirmation that msMRI can map neuronal activity in the human brain at high temporal and spatial resolution.

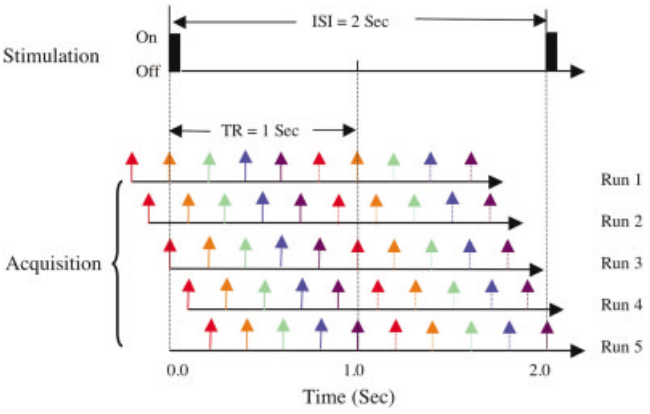

Figure 1.
The time sequence of experimental setups. Two five-slice images were acquired for each stimulation ON–OFF cycle. Each slice was color-coded. The time between adjacent slices was 200 msec. MRI scanner was precisely synchronized with stimulation onset. Data acquisitions for the first five runs started at −200, −100, 0, 100, and 200 msec relative to stimulation onset. The image acquired early (solid arrows) was contrasted with the image acquired later (dash arrows).

SUBJECTS AND METHODS

Subjects

Seven right-handed, healthy subjects (five men, two women) participated in this study. One data set was discarded due to motion artifacts. Three (of the six) were scanned twice at 1-week intervals to assess the reproducibility of the msMRI signal. Informed consent was obtained before each subject was imaged. For all studies, the head was immobilized in a closely fitted, thermally molded, plastic facial mask that was individually made for each subject. The mask minimized head movement during MRI scanning.

Paradigm

A well-established visuomotor task was used to investigate the system-level organization of the human visual and motor cortices using msMRI. Cued by a brief (50 msec) visual stimulus (a wedge of random dots) in the lower left visual field, subjects pressed and released a button with the right index finger.

Data acquisition

MRI data were acquired on a 1.9 T GE/Elscint Prestige whole-body MRI scanner using a gradient-echo echo-planar-image (EPI) pulse sequence with the following parameters: repetition time, TR, of 1,000 msec, echo time, TE, of 100 msec, and a flip angle of 90 degrees. Five contiguous, oblique slices were acquired, with an in-plane spatial resolution of 3×3 mm^2 and slice thickness of 6 mm. The orientation and location of the slices were carefully selected to cover both the upper bank of the calcarine cortex (the lower field representation of primary visual cortex) and the hand area of primary motor cortex. At the end of fMRI data collection, spin-echo, T1-weighted anatomical images in the same slice positions were acquired to facilitate the precise determination of the structures corresponding to the functional activation foci. The parameters for the T1-weighted images were: TR = 650 msec, TE = 12 msec, flip angle = 90 degrees, voxel size = $1.64 \times 1.64 \times 6$ mm^3.

Magnetic source MRI data were acquired as a contiguous series of 100 msec frames time-locked to cue onset (Fig. 1). Each MRI session included six runs of data acquisitions, with an acquisition time of 200 sec/run. The first five runs were designed for msMRI imaging of event-related neuronal activity and were shown in the schematic. Each run consisted of 100 ON/OFF cycles, with two five-slice images for each cycle (one ISI). MRI scanner was precisely synchronized with stimulation onset. Data acquisitions for the first five runs started at −200, −100, 0, 100, and 200 msec relative to stimulation onset. The image acquired early in the cycle (solid arrows) was contrasted with the image acquired later (dash arrows). The last run

was a control. It was acquired either at the resting-state (subject does not actively perform any task) or as a "traditional" block design blood oxygen level dependent (BOLD) fMRI study [Kwong et al., 1992; Ogawa et al., 1992], in which subjects carried out the visuomotor task for the first 90 sec and then rested for the rest of time. The block design BOLD fMRI data were acquired for three subjects with parameters of TR = 1,000 msec, TE = 45 msec, and flip angle = 90 degrees. Resting-state fMRIs were acquired for the other three subjects to assess false activation (noise). Parameters for the resting state MRI were TR = 700 msec, TE = 45 msec, and flip angle = 70 degrees.

Data analysis

The MRI images were processed using in-house software. The first 20 images of each run were discarded to allow hemodynamics and MRI signal to reach a steady state. All data were assessed for inter-scan and intra-subject movement. A two-dimensional (2-D) movement correction was carried out to minimize in-plane motion. Data interpolation between image slices was purposely avoided because different slices were acquired at different times. Voxel-by-voxel linear detrending was carried out to remove the linear drift of the MRI signal. A mean image was created for each ON–OFF cycle by averaging across the time-series in the cycle; the mean image was then subtracted from each image to create residual images. A 2-D spatial Gaussian filter with a full width at half magnitude of 4.5 mm was applied. A group Student's *t*-test was carried out on the residual images. The t-image was then thresholded using a *t*-value threshold of 3.0 ($P < 0.0013$) and cluster size threshold of six voxels to detect significant activation [Xiong et al., 1995, 1996].

Modeling

A current-dipole model, commonly used in MEG for the estimation of the magnetic fields induced by neuronal firing [Hobbie, 1997], was constructed for modeling MRI signal changes resulting from neuromagnetic fields. The model was constructed over a scale range from a single neuron to a typical MRI voxel (~1,000,000 neurons). Each dendrite was modeled as a current dipole. Distributions of neuronal magnetic fields were estimated and the interaction between the neuronal magnetic fields and nuclear spins was assessed across a range of scales, orientations, configurations, and distributions of dendrite packing density. More detailed information regarding modeling will be reported elsewhere.

RESULTS

As predicted, msMRI detected regional signal decrements in visual, sensorimotor, and pre-motor cortices with appropriate latencies, locations, and lateralities. Occipital activations bordered the calcarine fissure and were predominantly right hemispheric, consistent with the left visual field location of the cue. Similarly, sensorimotor and premotor activations were chiefly left hemispheric, consistent with the right-hand motor response. Primary motor area (M1) responses lay immediately anterior to the central sulcus; primary sensory cortex (S1) responses lay immediately posterior to the central sulcus. In all areas imaged, msMRI signals were detected predominantly in cerebral grey matter (Fig. 2). False-positive rate of activation was assessed based on the resting-state MRI data and was very low (<1%) for the present study. Trial-by-trial consistency was good (Fig. 2), with a clear distinction between baseline and activation. Visual inspections of activation maps showed good consistency across subjects and sessions. The locations of task-induced activations for msMRI and BOLD fMRI were also in good agreement in all subjects. As shown in the illustrated subject (Fig. 2), locations and lateralities of msMRI activations in M1, S1, the supplementary motor area (SMA) and posterior cingulate were closely replicated by BOLD fMRI.

In addition to spatial localization, msMRI maps provided useful temporal information regarding task-induced neuronal activity. As illustrated in Figure 2 (single subject) and in Figure 3 (group data), msMRI maps showed right-hemispheric activation of primary visual (striate) cortex (V1) in Frame 1 (0–100 msec) immediately after visual stimulation onset. The visual activation moved laterally to the right extrastriate visual areas (Brodmann area [BA] 18 and 19) in Frame 2 (100–200 msec). Both the striate and extrastriate visual cortical areas were re-activated in Frame 4 (300–400 msec). Onset latencies of msMRI visual activations agree well with the electroencephalography (EEG) literature, which reports onset latencies of 50–55 msec for striate cortex and 70–150 msec for extrastriate areas [Martinez et al., 1999; Woldorff et al., 1997]. Reentrant activation of visual cortex has also been reported, with onset at 250–300 msec, about 50 msec earlier than our result [Michel et al., 2001]. Note that our msMRI protocol measures integrated activation within a 100 msec frame (although shorter time frames are possible). Activation starting late in a frame may

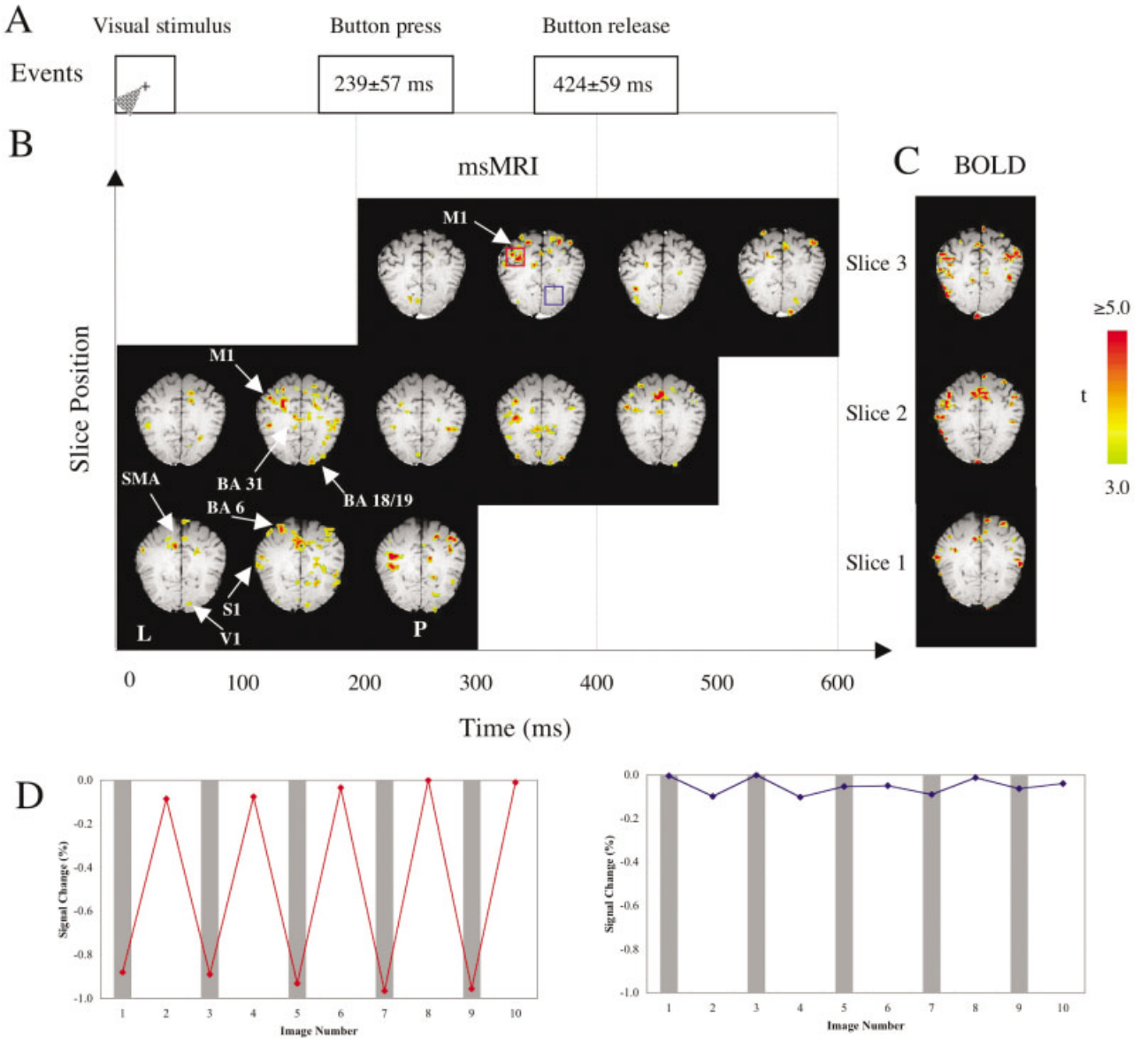

Figure 2.

Spatio-temporal plots of event-related neuronal activity detected by msMRI for a single subject. **A**: The time sequence of visual and motor events. **B**: Spatio-temporal plots of neuronal activity detected by msMRI. **C**: The same subject's BOLD fMRI maps. **D**: Time-course plots corresponding to the activated area (red box) and the non-activated area (blue box). The activation information (in color) is overlaid on T1-weighted MRI images acquired at the same location and orientation. Because different MRI slices were acquired at slightly different times, spatial normalization was not carried out to preserve temporal information. The color scale represents the *t*-value of each voxel. The letter L on the left-lower corner indicates the left cerebral hemisphere. The letter P indicates posterior. For the time-course plots, each data point here represents an average of 18 individual trials. The gray strips indicate stimulation ON.

not be detected until the subsequent frame, which may explain why activation onsets from EEG tend to be shorter than we observed with msMRI. The visual-area activation patterns illustrated in Figure 2 were fairly consistent across subjects and sessions. Group data (in the visual system) showed very little intersubject variability in response latency, making the group data quite similar to the single subject data (Fig. 3); this was not the case for brain regions affected by inter-subject differences in reaction time (below).

In the motor system, as well, msMRI detected activation spatially and temporally discrete and appropri-

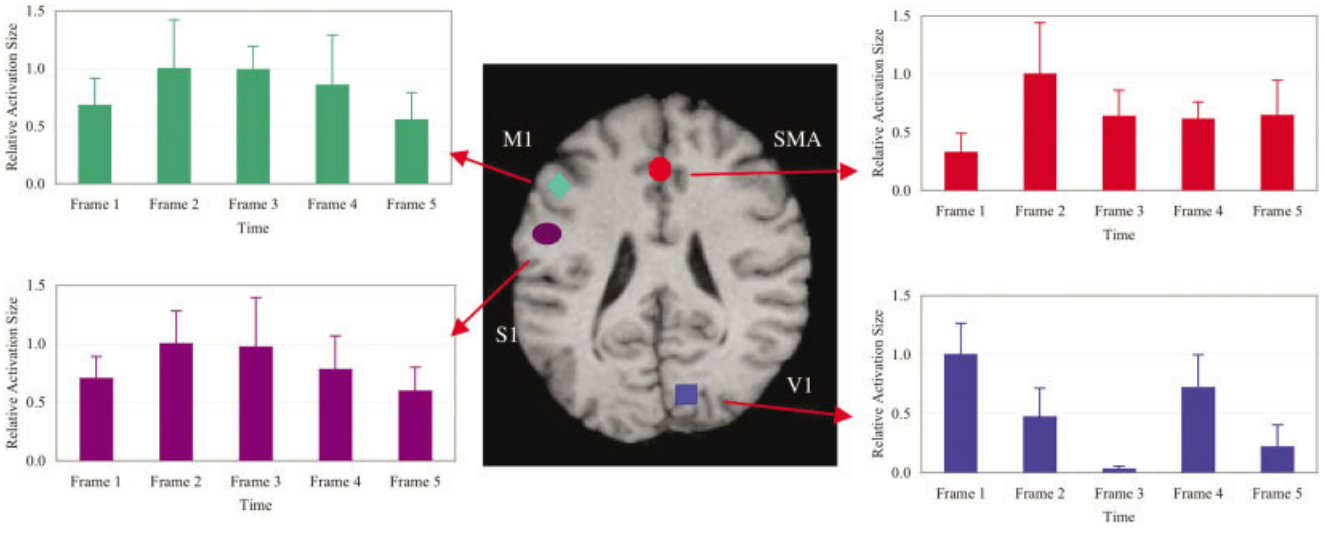

Figure 3.

Relative activation areas for different brain regions. Activation areas have been averaged across subjects and sessions and have been normalized by dividing each area by the maximum area for the region. Four different brain regions are shown: the right striate cortex (V1), the left primary motor and premotor cortices (M1), the left somatosensory cortex (S1), and the anterior supplementary motor area (SMA). Kolmogorov-Smirnov tests showed that the profile of M1 activation differs significantly from the profiles of V1 and SMA ($P < 0.01$) and is similar to that of S1 ($P = 0.05$). Time frames 1–5 represent time intervals of 0–100 msec, 100–200 msec, 200–300 msec, 300–400 msec, and 400–500 msec after the visual stimulation onset, respectively. Error bars = 1 SE.

ate to the task. The left primary motor (M1) and premotor areas (BA 6) were activated twice: first in Frame 2 (100–200 msec) and then in Frame 4 (300–400 msec) (Fig. 2). The first M1 activation is likely preparation for and execution of the button press. Using a similar visuomotor task, onset latencies of 130–180 msec have been reported for motor and premotor cortices, in excellent agreement with our data [Schluter et al., 1999]. The second M1 activation likely represents the same components for button release. Chronometric measurements showed an average delay of 185 msec between button press and button release, which closely matches the delay between the first and second M1 activations. As expected, the onset of brain activation preceded finger movement by about 100 msec (finger response time: 239 ± 57 msec). Similar onset latencies for button press and button release were observed in the group data (Fig. 3). Group data, however, also showed activation in Frame 3 as well as in Frames 2 and 4. Variability of reaction time between subjects is the most likely cause for this temporal smoothing of the group data. The supplementary motor area (SMA), a medial component of BA6, showed a similar temporal pattern, being first activated before movement (0–100 msec) and reaching a maximum at movement onset (100–200 msec); SMA, however, showed residual activation through Frames 3–5.

Although it might be expected that somatosensory processing would begin only after movement onset, recent studies have demonstrated that somatosensory processing can precede motor processing for a visuomotor task [Thut et al., 2000], either anticipating the to-be-received proprioceptive signal (efference copy) or using current body posture to model the to-be-executed movement [Parsons et al., 1995]. As shown in Figure 2, primary somatosensory (S1) cortex activation (0–100 msec) precedes M1 activation, and continued during M1 activation (100–200 msec), but reached maximum after M1 activation (200–300 msec). That is, the maximum S1 activation occurred in the epoch appropriate for arrival of a post-movement proprioceptive signal from the periphery [Ball et al., 1999]. The left S1 was again activated during the button release period (at 300–400 msec). This pattern was similar across subjects, albeit with latency differences reflecting inter-subject differences in reaction time. As in the motor system, reaction-time variability temporally smoothed the group data (Fig. 3).

To further test our supposition that the signals detected by this method are the direct effects of neuronal magnetic fields, theoretical modeling was carried out and experimentally confirmed. A current-dipole model, commonly used in MEG for the estimation of the magnetic fields induced by neuronal firing [Hob-

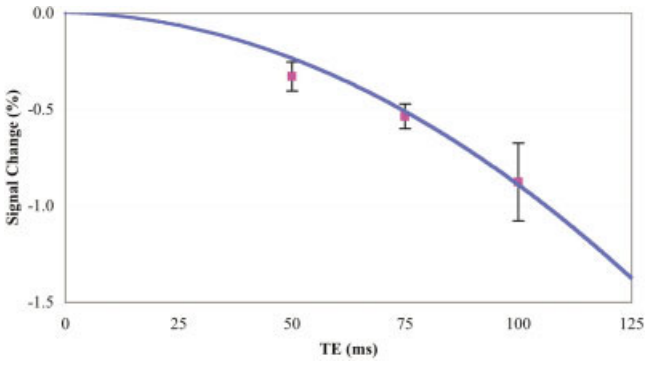

Figure 4.

TE dependence of msMRI signals. Theoretical modeling and additional scans of three subjects have been carried out to investigate effects of the echo time, TE, on msMRI signals. The solid line represents theoretical results. The symbols are experimental data, which represent the msMRI signals averaged across all significantly activated regions and across a group of three subjects. Error bars = 1 SE. The theoretical results were estimated based on a current dipole model. Parameters used for calculating the MRI signal changes are: radius of the dendrites $\alpha = 0.5$ μm, electrical conductivity of axoplasm $\sigma_i = 2\ \Omega^{-1}m^{-1}$, and membrane potential $\Delta v_i = 75$ mV [Hobbie, 1997]. The number of dendrites fired simultaneously at any time was presumed to be approximately 0.2 million for a typical MRI voxel. The plots show a non-linear relationship between the msMRI signals and the echo time TE. The data fit well with a quadratic model, in which msMRI signals are related to TE^2 ($r^2 = 0.9999$).

bie, 1997], was constructed over a scale range from a single neuron to a typical MRI voxel (~1,000,000 neurons). In the range of parameters proper for human cortex, our modeling showed that changes in the magnitude of the MRI signal due to neuronal activity could reach a few percent (0.5–5.0%). That is, msMRI signals are within a measurable range, comparable to standard fMRI techniques (Fig. 4). This theoretical prediction was confirmed by our experimental data (Figs. 2 and 4), which showed a signal change of 1.12% ± 0.54% of the background anatomical signal in left M1 cortex. Response magnitudes for other brain regions were similar.

Modeling also tested the relationship between the msMRI signal strength and the echo time (TE). A counterintuitive prediction of our model is that a non-linear relationship exists between TE and msMRI magnitude: msMRI signal increased by a factor of 3.8 when TE doubled. This is in sharp contrast to a nearly linear relationship between TE and BOLD fMRI signal. The predicted non-linearity was experimentally confirmed (Fig. 4). This is the reason why we use a long TE for msMRI.

DISCUSSION

This study showed that neuronal activity could be directly detected using MRI. In our experiment, msMRI detected responses localized to grey matter, appropriately lateralized, and with appropriate latency in visual, motor, and somatosensory brain regions, as predicted by task design and the electrophysiological literature. Signal strength of msMRI was comparable to traditional event-related functional MRI (fMRI) methods: about 1% of the baseline signal. Collectively, our observations demonstrate that the msMRI method achieved a temporal resolution (100 msec frames) exceeding that possible using MRI methods based on hemodynamics and metabolism and with no compromise of spatial resolution.

Prior efforts [Bodurka et al, 1999; Bodurka and Bandettini, 2002] to model the msMRI signal predicted a much weaker effect (one order of magnitude weaker) than predicted by our model. Their models were based on measuring phase rather than magnitude. This approach, we believe, is flawed. For neuronal magnetic fields, the direction of the field on the left side of a current dipole is always opposite to that on the right. A typical MRI voxel contains approximately a million dipoles. Both positive and negative phases of MRI signals will destructively add, lowering net phase for an imaging voxel. Thus, the net phase is near zero and is undetectable. On the other hand, magnitude of MRI signal significantly changes due to this neuromagnetic field. Even through millions of dendrites are synchronously activated, the combined magnetic field remains highly inhomogeneous. Nuclear spins experiencing these local field inhomogeneities will lose phase coherence, resulting in a decrease of MRI signal magnitude. Magnitude measurements used here, therefore, should be far more sensitive for measuring in vivo neuronal activity than phase measurements.

In addition to electromagnetic effects, neuronal activity also induces physiological (e.g., changes in blood flow and metabolic rate) and mechanical (e.g., cell swelling) effects. Is it possible that factors other than neuronal magnetic fields underlie our observations? A short answer is: unlikely.

Physiological and mechanical responses to neuronal activity have been characterized by numerous studies. Optical imaging studies [Gratton and Fabiani, 2001; Rector et al., 2001] have reported four distinct temporal components corresponding to neuronal activity: P30, N80, N300, and P800 responses. The two faster responses (P30, N80) were linked to cellular mechanical processes, such as cell swelling, which change the light-scattering properties of neural tissue. The timing

of the early positive response (P30) corresponds to the presynaptic population spike; the negative response (N80) corresponds to the postsynaptic population-evoked potential. The N300 response is believed to represent a fall in hemoglobin oxygenation, triggered by increased metabolic demand during activation. This component corresponds to the 'initial dip' in fMRI signal reported by several studies [Menon et al., 1995; Yacoub and Hu, 2001]. The P800 response corresponds to the hemodynamic BOLD fMRI effect.

The BOLD effect increases fMRI signal strength, whereas the msMRI effect causes a decrease. Thus, it is very unlikely that the observed effect is from BOLD. Further, the BOLD (P800) effect is a slow response, which typically peaks 5 sec or longer after stimulation onset and returns to baseline 15 sec or longer after stimulation offset. Our experiment was designed to minimize the effects of cerebral hemodynamics while maximizing the effects of neuronal magnetic transients, as the BOLD effect could cancel out the msMRI effect. The stimulation duty cycle (2 sec) was sufficiently rapid that the hemodynamical response was at steady state. Computer simulations ourselves and by others [Janz et al., 2001] demonstrate that effects of cerebral hemodynamics on the present experiment were negligible, being no more than 5% of the observed signal (0.05% of the baseline signal). Further, the high temporal resolution achieved in our msMRI-optimized paradigm could not possibly be achieved by the slow, hemodynamically based BOLD signal.

The "initial dip", an early decrease in the MRI signal, is believed due to a decrease in tissue oxygen content caused by a phase lag between the onset of neuronal metabolic demand (fast) and the onset of the hemodynamic response (slow) [Thompson et al., 2003]. The initial dip begins less than 1 sec after stimulation onset, peaks at approximately 2–3 sec, and merges with the BOLD effect at 4–5 sec [Yacoub and Hu, 2001]. The amplitude of this negative response is quite small: roughly 10% as large as the (positive) BOLD fMRI signal amplitude at 1.5 T and 30% at 4 T (20). At 1.9T (the field strength used here), the initial dip should be approximately 15% of the positive BOLD signal; our putative msMRI signal was comparable to the BOLD signal [Liu and Gao, 2000]. Thus, the initial dip is too small and too slow to be a plausible cause for the signals detected using our msMRI-optimized paradigm. Further, the initial dip occurs only at the onset of a stimulation block. In the block-like design used here, the transient oxygen debt was corrected (by the hemodynamic response) before data acquisition. Finally, even though the initial dip is faster than the BOLD signal in onset, it is slow in offset. The high temporal resolution (both onset and offset) achieved by our msMRI optimized paradigm could not be explained by the initial-dip effect.

Mechanical changes accompanying neuronal activation can generate extremely fast changes in MRI signals. In particular, firing-induced swelling of cortical cells (corresponding to P30 and N80 optical changes) is believed to change the apparent diffusion coefficient of water (ADC) and T_1 value of nuclear spins [Darquie et al., 2001]. In human visual cortex, visual stimulation induced a fast decrease in ADC with a magnitude similar to that observed here (~1%). The ADC effect, however, cannot explain the putative msMRI effect reported here for several reasons. First, a decrease in ADC causes an increase in MRI signal strength; the msMRI effect reported here is a decrease. Second, the ADC effect can be detected only when a strong diffusion gradient is applied. The pulse sequence we used was diffusion insensitive, in which no strong diffusion gradient was applied.

We believe, then, that the spatially and temporally precise signals detected using a model-based experimental design optimized to detect neuronal magnetic effects are, in fact, msMRI effects. The msMRI activations showed a spatial and temporal distribution appropriate to the neural systems activated by the widely used visuomotor task. The sign and magnitude of the observed signals (about −1% of baseline) were as predicted by the model. The nonlinear effect of TE on the observed signal was as predicted by the model. To the best of our knowledge, non-magnetic effects of neuronal activity have been addressed but found wanting as explanations of the observed effect.

The msMRI technique offers several advantages over current neuroimaging methods. It seems to provide better combined spatio-temporal resolution than any currently used non-invasive neuroimaging methods. Compared to "traditional" fMRI [Belliveau et al., 1991; Kwong et al., 1992] and positron-emission tomography (PET) [Fox et al., 1984, 1988; Mazziotta et al., 1982], msMRI offers much higher temporal resolution, with no loss of spatial resolution. Detecting brain activity via the cerebral hemodynamic and metabolic responses to neural firing, the temporal resolutions of fMRI and PET are ultimately limited by the slow response function of cerebral hemodynamics, which is on the order of seconds. Furthermore, their inferences regarding neuronal activity are necessarily complicated by the variability of coupling between neuronal activity, cerebral hemodynamics, and metabolism [Fox and Raichle, 1986]. Compared to EEG and MEG [Cohen, 1968; Lewine and Orrison, 1995], msMRI offers higher spatial accuracy. Relying on in-

formation detected at the scalp to localize active sites inside the brain, both EEG and MEG require solving an inverse problem, which leads to spatial uncertainty in the localization of electromagnetic sources. The msMRI effects are spatially mapped in the same manner as traditional MRI techniques and involve no inverse problem. In addition, EEG and MEG are each limited in the activation geometries they can detect and are unable to detect neuronal activities deep in the brain; msMRI has no such limitation. Combining information from modalities detecting different physiological variables (for example, data from fMRI and MEG) can partially offset the drawbacks of the individual modalities and can provide brain activation maps with high spatial and temporal resolution [Dale and Halgren, 2001]. The basic limitations for each modality, however, such as the indirect nature of a fMRI measurement and the inverse problems for EEG and MEG, remain obstacles. In contrast, msMRI overcomes these limitations and directly measures magnetic sources originating from the neural firing with high spatio-temporal resolution.

The temporal resolution of msMRI was 100 msec in this study. This temporal resolution, however, is still not optimal for investigating neuronal activity at the system level. Activation of a neural population generally lasts tens to hundreds of milliseconds. Similarly, latencies of activations are also in a range of tens to hundreds of milliseconds. Thus, improving the temporal resolution of msMRI would be valuable. Fortunately, the temporal resolution achieved here (100 msec) does not reflect a physical limitation of the msMRI method. The temporal resolution of msMRI is mainly limited by the echo time and contrast-to-noise ratio, which is affected by MRI parameters including field strength, repetition time, and echo time, as well as by the pattern of neural firing. Temporal resolution could be further improved by optimization of both experimental design and MRI pulse sequence.

ACKNOWLEDGMENTS

We thank Drs. G. Simpson and J. Lancaster for helpful discussions and C. Franklin, R. Perez, J. Roby, D. Fedrick, and Dr. J. Li for technical assistants. J.X. is financially supported by the National Science Foundation (BCS 0225711) and the National Institutes of Health (RO1 MH067163). J.H.G. is financially supported by the National Institutes of Health (AG19844 and RR17198).

REFERENCES

Ball T, Schreiber A, Feige B, Wagner M, Lucking CH, Kristeva-Feige R (1999): The role of higher-order motor areas in voluntary movement as revealed by high-resolution EEG and fMRI. Neuroimage 10:682–694.

Belliveau JW, Kennedy DN Jr, McKinstry RC, Buchbinder BR, Weisskoff RM, Cohen MS, Vevea JM, Brady TJ, Rosen BR (1991): Functional mapping of the human visual cortex by magnetic resonance imaging. Science 254:716–719.

Bodurka J, Bandettini PA (2002): Toward direct mapping of neuronal activity: MRI detection of ultraweak, transient magnetic field changes. Magn Reson Med 47:1052–1058.

Bodurka J, Jesmanowicz A, Hyde JS, Xu H, Estkowski L, Li SJ (1999): Current-induced magnetic resonance phase imaging. J Magn Reson 137:265–271

Cohen D (1968): Magnetoencephalography: evidence of magnetic fields produced by alpha-rhythm currents. Science 161:784–786.

Dale AM, Halgren E (2001): Spatiotemporal mapping of brain activity by integration of multiple imaging modalities. Curr Opin Neurobiol 11:202–208.

Darquie A, Poline JB, Poupon C, Saint-Jalmes H, Le Bihan D (2001): Transient decrease in water diffusion observed in human occipital cortex during visual stimulation. Proc Natl Acad Sci U S A 98:9391–9395.

Fox PT, Mintun MA, Raichle ME, Herscovitch P (1984): A noninvasive approach to quantitative functional brain mapping with H2(15)O and positron emission tomography. J Cereb Blood Flow Metab 4:329–333.

Fox PT, Raichle ME (1986): Focal physiological uncoupling of cerebral blood flow and oxidative metabolism during somatosensory stimulation in human subjects. Proc Natl Acad Sci U S A 83: 1140–1144.

Fox PT, Raichle ME, Mintun MA, Dence C (1988): Nonoxidative glucose consumption during focal physiologic neural activity. Science 241:462–464.

Gratton G, Fabiani M (2001): The event-related optical signal: a new tool for studying brain function. Int J Psychophysiol 42:109–121

Hobbie R (1997): Intermediate physics for medicine and biology. New York: Springer-Verlag. p 136–227.

Janz C, Heinrich SP, Kornmayer J, Bach M, Hennig J (2001): Coupling of neural activity and BOLD fMRI response: new insights by combination of fMRI and VEP experiments in transition from single events to continuous stimulation. Magn Reson Med 46: 482–486.

Joy M, Scott G, Henkelman M (1989): In vivo detection of applied electric currents by magnetic resonance imaging. Magn Reson Imaging 7:89–94.

Kamei H, Iramina K, Yoshikawa K, Ueno S (1999): Neuronal current distribution imaging using MR. IEEE Trans Magn 35:4109–4111.

Kwong KK, Belliveau JW, Chesler DA, Goldberg IE, Weisskoff RM, Poncelet BP, Kennedy DN, Hoppel BE, Cohen MS, Turner R, et al. (1992): Dynamic magnetic resonance imaging of human brain activity during primary sensory stimulation. Proc Natl Acad Sci U S A 89:5675–5679.

Lewine J, Orrison W (1995): Clinical electroencephalography and event-related potentials. In: Orrison W, Lewine J, Sanders J, Hartshorne M, editors. Functional brain imaging. New York: Mosby-Year Book, Inc. p 327–368.

Liu H, Gao J (2000): An investigation of the impulse functions for the nonlinear BOLD response in functional MRI. Magn Reson Imaging 18:931–938.

Martinez A, Anllo-Vento L, Sereno MI, Frank LR, Buxton RB, Dubowitz DJ, Wong EC, Hinrichs H, Heinze HJ, Hillyard SA (1999): Involvement of striate and extrastriate visual cortical areas in spatial attention. Nat Neurosci 2:364–369.

Mazziotta JC, Phelps ME, Carson RE, Kuhl DE (1982): Tomographic mapping of human cerebral metabolism: auditory stimulation. Neurology 32:921–937.

Menon RS, Ogawa S, Hu X, Strupp JP, Anderson P, Ugurbil K (1995): BOLD based functional MRI at 4 Tesla includes a capillary bed contribution: echo-planar imaging correlates with previous optical imaging using intrinsic signals. Magn Reson Med 33:453–459.

Michel CM, Thut G, Morand S, Khateb A, Pegna AJ, Grave de Peralta R, Gonzalez S, Seeck M, Landis T (2001): Electric source imaging of human brain functions. Brain Res Brain Res Rev 36:108–118.

Ogawa S, Tank DW, Menon R, Ellermann JM, Kim SG, Merkle H, Ugurbil K (1992): Intrinsic signal changes accompanying sensory stimulation: functional brain mapping with magnetic resonance imaging. Proc Natl Acad Sci U S A 89:5951–5955.

Parsons LM, Fox PT, Downs JH, Glass T, Hirsch TB, Martin CC, Jerabek PA, Lancaster JL (1995): Use of implicit motor imagery for visual shape discrimination as revealed by PET. Nature 375:54–58.

Rector DM, Rogers RF, Schwaber JS, Harper RM, George JS (2001): Scattered-light imaging in vivo tracks fast and slow processes of neurophysiological activation. Neuroimage 14:977–994.

Schluter ND, Rushworth MF, Mills KR, Passingham RE (1999): Signal-, set-, and movement-related activity in the human premotor cortex. Neuropsychologia 37:233–243.

Scott GC, Joy ML, Armstrong RL, Henkelman RM (1992): RF current density imaging in homogeneous media. Magn Reson Med 28: 186–201.

Thompson J, Peterson M, Freeman R (2003): Single-neuron activity and tissue oxygenation in the cerebral cortex Science 299:1070–1072.

Thut G, Hauert CA, Blanke O, Morand S, Seeck M, Gonzalez SL, Grave de Peralta R, Spinelli L, Khateb A, Landis T, Michel CM (2000): Visually induced activity in human frontal motor areas during simple visuomotor performance. Neuroreport 11:2843–2848.

Woldorff M, Fox P, Matzke M, Lancaster J, Veeraswamy S, Zamarripa F, Seabolt M, Glass T, Gao J, Martin C, Jerabek P (1997): Retinotopic organization of early visual spatial attention effects as revealed by PET and ERPs. Hum Brain Mapp 5:280–286.

Xiong J, Gao JH, Lancaster JL, Fox PT (1995): Clustered pixels analysis for functional MRI activation studies of the human brain. Hum Brain Mapp 3:287–301.

Xiong J, Gao J-H, Lancaster JL, Fox PT (1996): Assessment and optimization of functional MRI analyses. Hum Brain Mapp 4:153–167.

Yacoub E, Hu X (2001): Detection of the early decrease in fMRI signal in the motor area. Magn Reson Med 45:184–190.